NANO LETTERS

Letter

pubs.acs.org/NanoLett

Tunable Rashba Effect in Two-Dimensional $LaOBiS_2$ Films: Ultrathin Candidates for Spin Field Effect Transistors

Qihang Liu,*,† Yuzheng Guo,‡ and Arthur J. Freeman†

†Department of Physics and Astronomy, Northwestern University, Evanston, Illinois 60208, United States

‡Department of Engineering, University of Cambridge, Cambridge CB3 0FA, United Kingdom

ABSTRACT: Rashba spin splitting is a two-dimensional (2D) relativistic effect closely related to spintronics. However, so far there is no pristine 2D material to exhibit enough Rashba splitting for the fabrication of ultrathin spintronic devices, such as spin field effect transistors (SFET). On the basis of first-principles calculations, we predict that the stable 2D $LaOBiS_2$ with only 1 nm of thickness can produce remarkable Rashba spin splitting with a magnitude of 100 meV. Because the medium La_2O_2 layer produces a strong polar field and acts as a blocking barrier, two counter-helical Rashba spin polarizations are localized at different BiS_2 layers. The Rashba parameter can be effectively tuned by the intrinsic strain, while the bandgap and the helical direction of spin states sensitively depends on the external electric field. We propose an advanced Datta-Das SFET model that consists of dual gates and 2D $LaOBiS_2$ channels by selecting different Rashba states to achieve the on−off switch via electric fields.

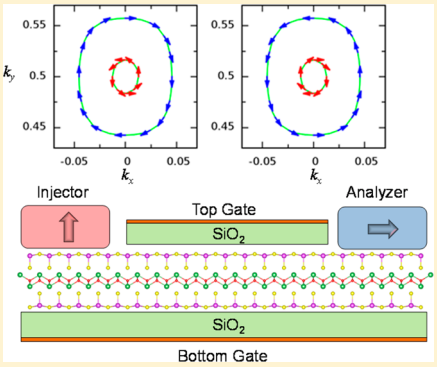

KEYWORDS: *Rashba effect, spin field effect transistor, two-dimensional $LaOBiS_2$, biaxial strain, electric field, density functional theory*

Spin−orbit coupling (SOC), a relativistic effect in electron systems, creates an effective magnetic field and thus lifts the spin degeneracy in periodic solids.[1,2] Among the effects of SOC, Rashba spin splitting, which originates from the potential gradient induced by the structural inversion asymmetry (SIA), attracts much interest due to its electric tunability and potential applications, such as spin field effect transistors (SFETs).[3,4] The Rashba-type interaction is described by a linear-momentum Hamiltonian,

$$H_R = \lambda(\nabla V \times \boldsymbol{p})\cdot\boldsymbol{\sigma} = \alpha_R(\sigma_x k_y - \sigma_y k_x) \quad (1)$$

where ∇V, $\boldsymbol{p}$, and $\boldsymbol{\sigma}$ denote potential gradient, electron momentum, and Pauli matrix vector $(\sigma_x,\sigma_y,\sigma_z)$ respectively. The consequence of eq 1 is two spin polarized dispersions, with a momentum offset characterized by the Rashba parameter α_R, forming helical spin states. Typical Rashba splittings with the order of millielectronvolts are found in semiconductor heterostructures, including AlGaAs/GaAs and InAs/GaSb quantum wells,[5,6] and are further realized at the heavy-metal surface states, such as Au(111)[7] and Bi(111),[8,9] by using spin-, angular-resolved photoemission spectroscopy (SR-ARPES). In order to obtain more significant spin splitting, particular experimental and theoretical efforts focus on the noble-metal surface alloys, like Bi−Ag(111)[10] and Bi−Si(111).[11] However, when considering possible applications, semiconducting structures with large Rashba effect are more desirable because of their manipulability under gate voltages.[12]

Recently, a giant bulk Rashba effect was found in the polar semiconductor BiTeI.[13] The spin splitting originated from the layered configuration, similar to a 2D electron system. Because of the robustness and straightforward fabrication process, the interest of Rashba splitting from this mechanism is growing steadily.[14−17] However, the ionic bonding between layers hinders the formation of stable freestanding thin films, which is highly desirable for circuit integration. Therefore, stable thin films with relatively large Rashba splitting are still under extensive exploration.

Since the discovery of graphene,[18] the milestone of the two-dimensional (2D) material, many efforts focus on such 2D carbon network and their analogs like silicene and germanene[19] due to their exotic properties such as high mobility and long spin lifetime.[19−23] However, the light atoms determine the magnitude of the SOC effect to be quite small in such materials (10^{-3} and 1 meV for graphene and silicene, respectively),[21,22] which is far from the requirement of SFET under a reasonable external field. Another kind of 2D material, the inversion-asymmetric monolayer MoS_2, also arises intense attention by its ideal performance in valley polarization.[24−26] However, the spin splitting in MoS_2 is also not large enough to make the channel below the coherence transport limit. Therefore, although many 2D materials exhibit intriguing spintronic properties, there is still no stable 2D material with large Rashba spin splitting for SFET applications.

Here, by using first-principles calculations, we predict that the 2D form of $LaOBiS_2$ can produce a remarkable Rashba spin splitting with a magnitude of 100 meV. Meanwhile, the thickness of the system is down to 1 nm, much thinner than the Rashba materials with comparable spin splitting ever reported.

Received: July 23, 2013
Revised: September 27, 2013
Published: October 15, 2013

Our formation energy and phonon spectrum calculations predict that $LaOBiS_2$ can be stable in a free-standing single-slab structure, illustrating its promising application to the next-generation spintronic devices, especially SFET. The Rashba splitting derives from the strong polar field from La_2O_2 to the BiS_2 layers. Owing to the global inversion symmetry, there are two counter-helical Rashba spin polarizations localized at two BiS_2 layers with weak interaction. Thus, a small electric field or substrate can induce the broken symmetry and thus obtain two sets of spin splittings. Furthermore, we also use two methods to investigate the modulation of the electronic and spintronic properties of such 2D systems, including intrinsic strain and external electric field, and reveal that the property related to the Rashba effect is sensitive to the internal atomic interaction, while the main effect of the electric field is tuning the bandgap continuously by a rigid band shift. Finally, by selecting different Rashba states to control the on−off switch via electric fields, we propose an advanced Datta-Das SFET model which consists of dual gates and the 2D $LaOBiS_2$ channel.

$LaOBiS_2$ is one of the BiS_2-based layered compounds recently discovered to have similar properties with cuprate and iron-based superconductors.[27−31] Bulk $LaOBiS_2$ possesses a ZrCuSiAs-type crystal structure and a *P4/nmm* symmetry with an inversion center located at the center of two nonequivalent O atoms. Its unit cell has a triple-layer (TL) structure with a La_2O_2 layer sandwiched between two BiS_2 layers, as shown in Figure 1a,b. The van der Waals force

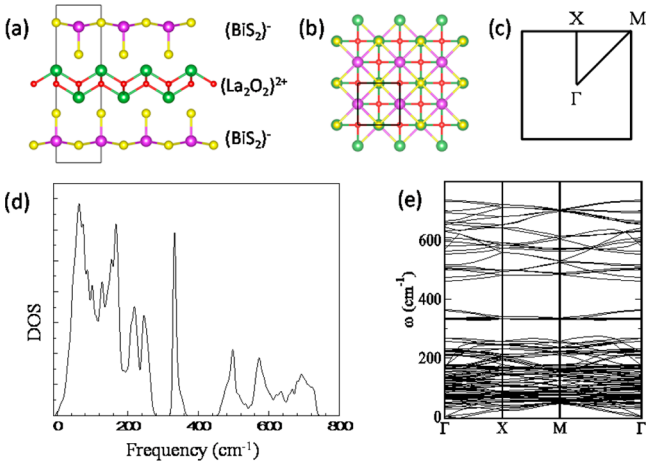

Figure 1. (a) Side view and (b) top view of the crystal structure of the 1-TL slab $LaOBiS_2$, the triple-layer unit is shown in the black frame. The green, red, purple, yellow balls represent La, O, Bi, and S atoms, respectively. (c) The 2D Brillouin zone of the corresponding rectangular structure. (d) Phonon density of states (DOS) and (e) phonon dispersion of the 1-TL slab $LaOBiS_2$.

dominates the interaction between two adjacent BiS_2 layers so that bulk $LaOBiS_2$ is formed by weakly coupling 2D TL slabs, indicating that the stable 2D $LaOBiS_2$ is possible to fabricate by the exfoliation, vapor deposition, or molecular-beam epitaxy. The great performance and unique properties of monolayer MoS_2 in nanoelectronic devices stimulates the discovery of 2D transition metal oxides and dichalcogenides.

Recent experimental and theoretical studies predicted that, many layered MX_2 materials (M, transition metal; X, chalcogen atom) with strong covalent in-plane bonds and weak van der Waals-like coupling between layers can be made into stable single-layer structures.[20,21] Likewise, here we use the following formula to calculate the formation energy

$$E_{for} = \frac{[E_c(LaOBiS_2) - E_c(La) - E_c(O) - E_c(Bi) - 2E_c(S)]}{N_{atom}} \quad (2)$$

where E_c denotes the cohesive energy relative to free constituent atoms, and N_{atom} is the number of a $LaOBiS_2$ primitive cell. The calculated formation energy of monolayer $LaOBiS_2$ is −1.40 eV/atom, lower than most of the MX_2 monolayers (for example, the corresponding theoretical value in some famous MX_2 compound like MoS_2, WS_2, and $NbSe_2$ are 0.83, 0.91, and 0.88 eV/atom, respectively).[32] Moreover, the binding energy of the 1-TL slab to its bulk phase is −86 meV/atom, while the counterpart of MoS_2 is −73 meV/atom according to our calculations for which the order implies weak van der Waals interactions.[33]

In order to further provide a rigorous test for the dynamic stability, we also calculated the phonon spectrum of 1-TL $LaOBiS_2$. The phonon DOS and the corresponding band dispersion are shown in Figure 1d,e, respectively. It is clearly seen that all the branches have positive frequencies with no imaginary phonon modes, confirming the dynamic stability of the sandwich system. It is noticeable that in some previous work the phonon dispersion of 3D $LaOBiS_2$ shows an unstable region around M (1/2, 1/2) point by 1 × 1 primitive cell calculation (reciprocal grid shown in Figure 1c).[30,31] It is because of the additional constrains imposed by the periodic boundary condition used in these calculations. We observed the similar negative frequency in our primitive cell calculation. To avoid it we use the 2 × 2 supercell without further geometry relaxation, which does not change the atomic structure but provides a more generalized boundary condition compared with the primitive cell. It is confirmed that the 2 × 2 boundary condition can stabilize the lowest phonon modes. As a result, both 3D and 2D $LaOBiS_2$ are predicted to be stable. The stability analysis discussed above and the advancing experimental techniques make us more confident to believe that such a 1-TL slab $LaOBiS_2$ can form a thermodynamically stable 2D structure, which calls for further experimental investigations.

The electronic properties of 1-TL $LaOBiS_2$ are shown in Figure 2. Without SOC, the band structure shows a semiconductor nature with a direct bandgap located at X (0, 1/2). By projecting the bands onto different atomic orbitals we find that the low energy spectrum near the Fermi level mainly comes from the BiS_2 layers (see Figure 2a). Therefore, the sandwich structure behaves like a mini "quantum well", with the La_2O_2 layer as a potential barrier preventing wave function overlap of the BiS_2 layers. Along Γ-X, both of the two highest valence bands (HVB-1, 2) and the two lowest conduction bands (LCB-1, 2) are nearly 2-fold degenerate (excluding spin). This is because the interaction between two BiS_2 layers is insignificant due to the existence of the blocking layer (BL) La_2O_2, and the two HVBs (LCBs) are easily distinguished by the contribution of different BiS_2 layers, which is important for the preservation of the properties of each layer. The real-space charge density of the maxima of two HVBs shown in Figure 2e reveals a domination of Bi-s and S-p states with invisible contribution of La_2O_2 layers. The corresponding density distribution along the *z* direction (Figure 2d) indicates that the two HVBs are localized at the top and bottom BiS_2 layers,

dx.doi.org/10.1021/nl4027346 | *Nano Lett.* 2013, 13, 5264−5270

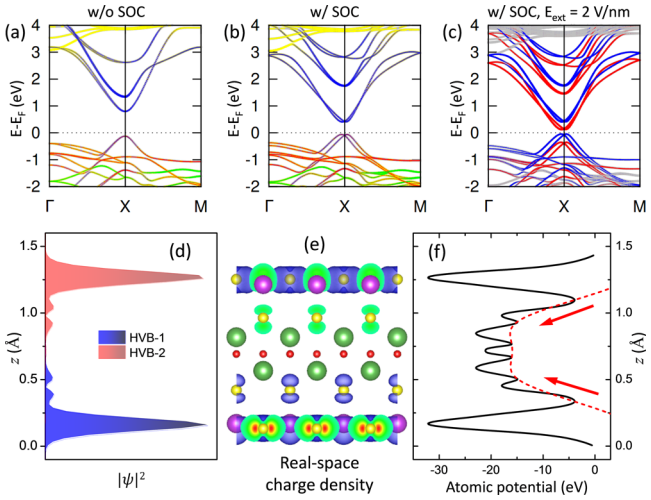

Figure 2. Band structures with atomic projection of the 1-TL $LaOBiS_2$ (a) without SOC, (b) with SOC, and (c) with SOC and an external electric field of 2 V/nm. In panels (a,b), the atomic characters La, O, Bi, and S are indicated by yellow, green, blue, and red, respectively. In panel (c), red and blue denote top and bottom BiS_2 layers, respectively. (d) The charge density integrated over the 2D plane and (e) the real-space charge density distribution of the maxima of the two HVBs. (f) Atomic local potential (black solid) and the corresponding envelope profile (red dash) along the z direction. The two opposite intrinsic polar fields are explicitly indicated by red arrows.

respectively. Moreover, the symmetry character of the nonsymmophic space group *P*4/*nmm* makes the whole X-M path 2-fold degenerate.

Besides acting as a blocking barrier, the La_2O_2 layer has another role as a polarized medium providing ionic bonding with the BiS_2 layers. As a result, the BiS_2 layers feel strong polar fields with opposite directions that make themselves individual Rashba layers (RLs). The whole system becomes a stacking bilayer structure with two counter-helical RLs, or more precisely, an RL-BL-RL sandwich system. From the envelop plot of the atomic local potential along the z direction, as shown in Figure 2f, we can easily observe the evidence of two polar fields produced by the ionic bonding. Recently, many novel phenomena related to spintronics are uncovered in such a Rashba bilayer system, such as "home-made" topological insulator[34] and topological superconductivity.[35] Most of the proposals are based on the symmetric heterostructures fabricated by surface growth techniques like beam epitaxy. Here we predict 1-TL $LaOBiS_2$ as a pristine Rashba bilayer system. The little coupling between two RLs preserves two sets of Rashba spin splitting, which ensures a promising candidate for the SFET devices.

As shown in Figure 2b, with SOC turning on both the LCB and HVB experience significant splitting. This Rashba-like band splitting is unusual for such a centrosymmetric system because the Rashba splitting results from the SIA. However, although the thickness of 1-TL $LaOBiS_2$ is only 1 nm, there are two strong polar fields from the BL to the two RLs, or in other words, two local SIAs. Therefore, the two SIAs with little interaction between each other ensure two counter-helical Rashba states localized at the top and bottom BiS_2 layers. The two sets of spin splitting are doubly degenerate in energy owing to the global inversion symmetry. We further plot the spin textures in the vicinity of X in order to analyze the character of the spin splitting. In the HVB, we find opposite spin helical states localized on BiS_2 layers with nearly zero S_z component, which is the fingerprint of pure Rashba splitting (see Figure 3b). The energy contour shows a little ellipse character, due to

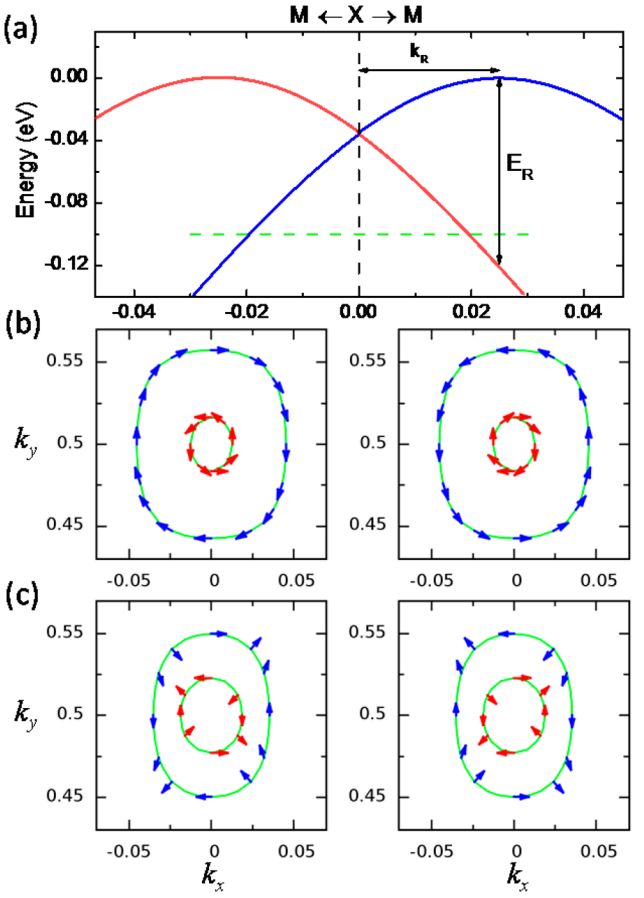

Figure 3. (a) A scaled-up view of the Rashba splitting at the valence band maximum of 1-TL $LaOBiS_2$. In-plane spin texture (blue and red arrows) on the energy contour (green line) (b) 100 meV below the valence band (green dashed line marked in panel (a)), and (c) 100 meV above the conduction band minimum.

the extra splitting caused by residual interaction between BiS_2 layers along the Γ-X direction, while such an interlayer interaction vanished along X-M due to the symmetry constrain. On the other hand, the spin patterns of the LCB behave like a combination of Rashba and Dresselhaus splitting, as shown in Figure 3c. We know that the Rashba splitting originates from the local dipole field, which also induces the inversion asymmetry, and thus leads to Dresselhaus splitting, depending on the symmetry of the specific bands as well. The HVB-1,2 belongs to X_2, which makes the Dresselhaus splitting vanish; while the LCB-1,2 belongs to X_1, which makes the matrix element of the Dresselhaus term nonzero, indicating a hybridization of different spin splitting and a more complicated spin texture.

The pure Rashba spin splitting for the hole carriers is also of great importance for the spintronic transport in devices. A scale-up scheme for the HVBs with the parameters related to the Rashba effect is shown in Figure 3a. The spin splitting energy E_R is 119 meV, whereas the corresponding momentum offset k_R = 0.025 Å^{-1}. Hence we can evaluate the Rashba parameter $\alpha_R = E_R/k_R$ = 4.78 eV·Å. This magnitude of the spin

dx.doi.org/10.1021/nl4027346 | *Nano Lett.* 2013, 13, 5264−5270

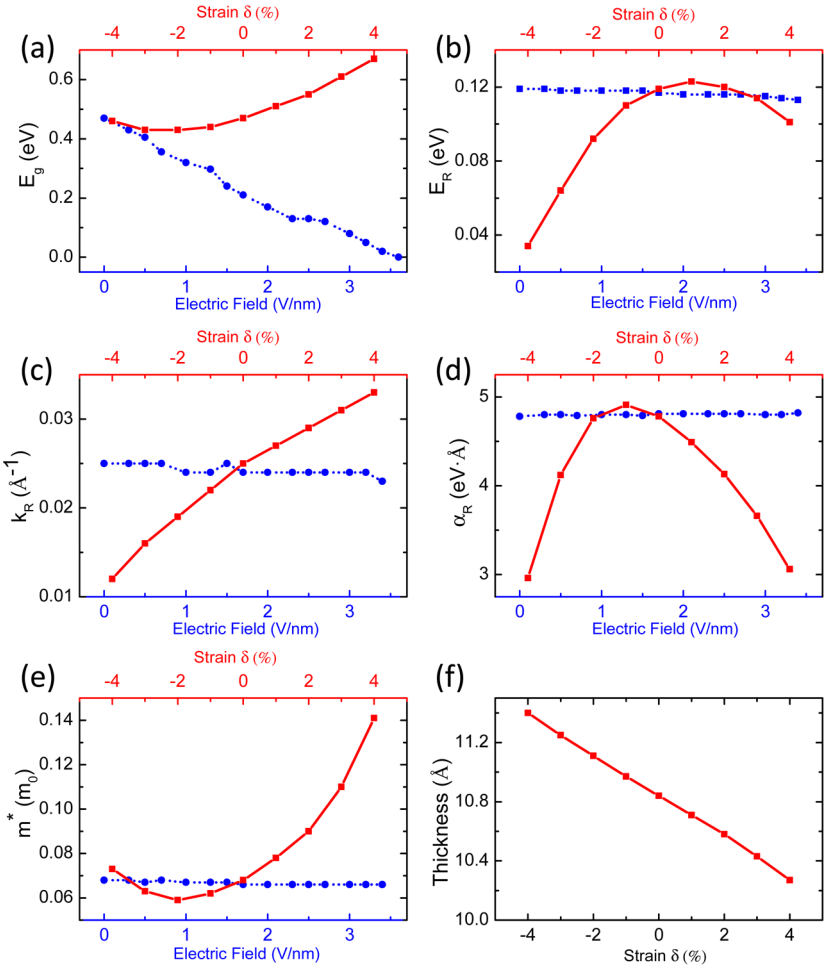

Figure 4. (a) The intrinsic strain (squares with red solid line) and external electric field (circles with blue dotted line) dependencies of the electronic and spintronic quantities in 1-TL $LaOBiS_2$: (a) bandgap; (b) Rashba splitting energy; (c) the corresponding momentum offset; (d) Rashba parameter; (e) effective mass; and (f) the thickness of 1-TL slab.

splitting is among the largest counterparts ever found,[10,13,15,17] and 2 orders larger than the ultrathin 2D Rashba structures such as graphene or MoS_2. A larger Rashba splitting energy E_R is desirable for stabilizing and controlling spin while a larger momentum offset k_R is advantageous for achieving a significant phase offset for different spin and thus favorable for the spin transport. Therefore, for potential applications it is obviously of particular interest to increase some of the Rashba parameters E_R, k_R, and α_R. It is well-known that there are two effective methods to tune the Rashba parameters, hydrostatic stains to intrinsically change the interatomic bonding and an external electric field perpendicular to the 2D plane. In the following, we will apply these two methods on 1-TL $LaOBiS_2$ to examine the modulation of the electronic structure and Rashba properties.

First, we impose biaxial strain on the 2D plane of 1-TL $LaOBiS_2$ by tuning the planar lattice parameter a. After applying the strain, all the atoms are fully relaxed. The magnitude of the strain is described by $\delta = (a - a_0)/a_0$, where a_0 = 4.037 Å is the planar lattice constant without strain. Figure 4 shows that all the quantities of interest are modified significantly by the biaxial strain (squares with red solid line), implying that the interatomic coupling can drastically tune the internal potential gradient of 1-TL $LaOBiS_2$, and thus modulate the electronic and spintronic properties. In detail, the bandgap (E_g, in Figure 4a) and effective mass (m^*, in Figure 4e) share the similar trend in the range from $\delta = -4\%$ to 4%, that is, reaching the minimum at $\delta = -2\%$ and then keep increasing. E_g changes from 0.43 eV at $\delta = -2\%$ to 0.67 eV at δ =4% by 56% increase, while m^* changes from 0.059 m_0 at $\delta = -2\%$ to 0.141 m_0 a δ = 4%t by 139% increasing. On the other hand, E_R increases from 34 meV at $\delta = -4\%$ to a maximum of 123 meV at $\delta = -2\%$. The remarkable reduction of E_R after 123 meV with the compressive strain is probably because atoms begin to relax toward the z direction under pressure. As a result, the thickness of the monolayer becomes larger and thus weakens the built-in polar field and the Rashba splitting (see Figure 4f). The momentum offset k_R increases monotonically with the biaxial strain within the range of $\delta = -4$ to 4%. More importantly, we notice that when the material sustains a compressive strain, both E_R and k_R are reduced, which is adverse to the technological applications. Meanwhile, for the tensile strain one can effective enhance k_R while maintaining the splitting energy over 100 meV. The Rashba coefficient α_R reaches the maximum of 4.91 eV·Å at $\delta = -1\%$. In a word, the flexible modulation of the spin splitting of 1-TL $LaOBiS_2$ offers a route to engineer the Rashba SOC by biaxial strain for the benefit of spintronic devices.

Next, we have also investigated the dependence of the electronic and spintronic character on the external electric field E_{ext}, which is mostly considered for modulate the performance

dx.doi.org/10.1021/nl4027346 | Nano Lett. 2013, 13, 5264−5270

of the Rashba devices.[4,36] The external electric field usually induces two effects on low-dimensional systems, tuning the Rashba parameters by modifying the SIA, and the bandgap modulation by the well-known Stark effect, which has been observed in many previous studies on BN ribbons and MoS_2 sheets.[37,38] When applying an external electric field perpendicular to the 2D plane, the degenerate Rashba-like bands begin to split owing to the Stark effect, as shown in Figure 2c. The vertical electric field induces a potential difference between the two BiS_2 layers, which is responsible for the band separation. Therefore, opposite helical spin states corresponding to top and bottom BiS_2 layers are separated not only spatially but also energetically. By comparing Figure 2b,c, we notice that the dominating effect of E_{ext} is separating the degenerate levels belonging to different layers from each other, while the shape of the Rashba bands remain nearly the same as the case without E_{ext}. The remarkable E_R and k_R still originate from the local inversion asymmetry of the sandwich structure of 1-TL $LaOBiS_2$.

The bandgap, effective mass, and the Rashba parameters as a function of E_{ext}, are also shown in Figure 4 for comparison with the biaxial strain. We find that by applying E_{ext}, the modulation of the bandgap is even more significant than that under strains. The Stark energy splitting caused by the potential difference is approximately expressed as $E_S = -dE^*e$, where E^* is the screened electric field and d is the distance of the BiS_2 layers. Therefore, the larger E^*, the larger E_S is, and thus the smaller bandgap. As a result, the bandgap decreases monotonically with the electric field and falls to zero eventually under a critical field of 3.6 V/nm, as shown in Figure 4a. In sharp contrast, the Rashba parameters and the hole effective mass remain nearly unchanged compared with the intrinsic modulation, which contradicts the conventional sense that the Rashba effect can be effectively tuned by E_{ext}. The reason lies in that in such a bulk-induced Rashba system as $LaOBiS_2$ and BiTeI, the huge Rashba parameter makes the effect of E_{ext} seem insignificant. The modulation of the Rashba parameter α_R in 1-TL $LaOBiS_2$ is the order of 10^{-2} eV·Å under E_{ext} of 1 V/nm (from 4.78 to 4.82 eV·Å within the 0−3.6 V/nm range), which is similar with the traditional Rashba systems based on semiconductor heterostructures.[6,39] However, the spin splitting in $LaOBiS_2$ and BiTeI originates from the polar field induced by the strong ionic bonding between atoms. By measuring the slopes of the atomic potential envelope shown in Figure 2f, we estimate that the intrinsic polar fields from the La_2O_2 layer to both BiS_2 layers to be 74.7 V/nm, which is much larger than the external field we applied. Therefore, although a reasonable E_{ext} can close the bandgap of 1-TL $LaOBiS_2$, it cannot enhance or diminish the polar field sufficiently to change the Rashba spin splitting. This is also evidence that the bulk-induced Rashba systems can generate much larger Rashba splittings than the conventional Rashba systems caused by E_{ext}.

It is reported that the bandgap narrowing can further enhance the Rashba spin splitting in the bulk BiTeI[40,41] due to the second-order $\boldsymbol{k}\cdot\boldsymbol{p}$ perturbative correction of the SOC term $\Delta\varepsilon_m^{(2)}(k) \propto \sum_{n\neq m}([\lambda_k\langle u_m|(\nabla V \times \boldsymbol{p})\cdot\boldsymbol{\sigma}|u_n\rangle + c.c.]/(\varepsilon_m - \varepsilon_n))$, where u_i and ε_i denote the eigenstate and eigenvalue of the state i. The LCB and HVB states in BiTeI are symmetrically of the same character, which makes the SOC matrix element $\langle u_m|(\nabla V \times \boldsymbol{p})\cdot\boldsymbol{\sigma}|u_n\rangle$ nonzero, and thus lead to an effective coupling to attract each other. However, in the 1-TL $LaOBiS_2$, the different symmetric character of LCB and HVB cause $\langle u_m|(\nabla V \times \boldsymbol{p})\cdot\boldsymbol{\sigma}|u_n\rangle$ to be symmetrically prohibited so that there is no second-order coupling that depends on the narrowing bandgap. Therefore, the Rashba parameters remain unchanged even when the bandgap is closed under the critical E_{ext}, as we found in Figure 4.

It is well-known that bandgap engineering is a powerful technique for improving the performance of candidate materials to meet the requirements of nanoelectronic devices; for example, the electric control of bilayer graphene sheets.[42] Compared with a single-gated FET, a dual-gated device can not only tune the vertical electric field applied on the channel, but also the doping level.[23] Here we propose a dual-gated SFET composed of the 2D $LaOBiS_2$ as the channel, as shown in Figure 5a. The injector and analyzer are ferromagnetic

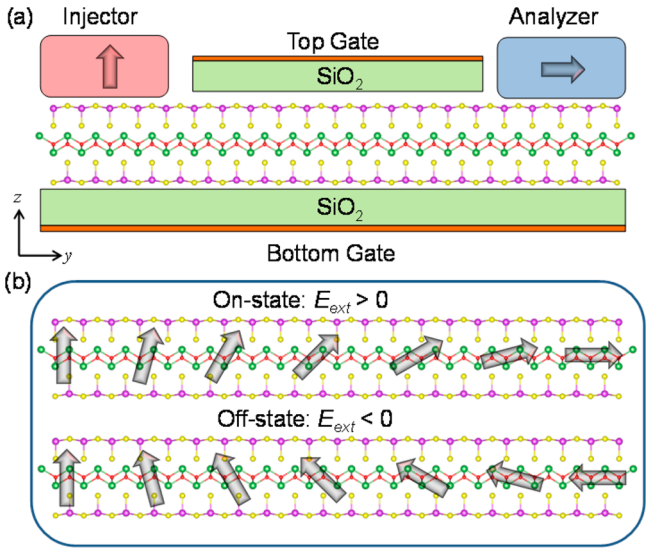

Figure 5. (a) Schematic model of dual-gated spin field effect transistor based on the ultrathin $LaOBiS_2$ channel and two ferromagnetic electrodes. (b) The spin precession (indicated by arrows) in on- and off-states by reversing the external electric field.

electrodes with their spin polarization perpendicular to each other. We assume that the channel is along the y direction so that the electron in the vicinity of X point with a wave vector $(0, k_y, 0)$ can travel through it. Then according to eq 1, with a positive E_{ext}, the Rashba states in the $LaOBiS_2$ channel are

$$\psi_{\pm}(\boldsymbol{k}) = \frac{1}{\sqrt{2}}e^{i(k_x x + k_y y)}\begin{pmatrix}1\\ \mp ie^{i\varphi}\end{pmatrix} = \frac{1}{\sqrt{2}}e^{ik_y y}\begin{pmatrix}1\\ \pm 1\end{pmatrix} \quad (3)$$

where φ is the azimuth angle of electron momentum $\boldsymbol{k}$ in the xy plane. If we pick the spin polarization of the injector along $+z$ direction, the propagating wave function in the channel is written by the entanglement of the Rashba states

$$\psi_c(\boldsymbol{k}) = \frac{1}{2}\left[e^{ik_1 y}\begin{pmatrix}1\\ 1\end{pmatrix} + e^{ik_2 y}\begin{pmatrix}1\\ -1\end{pmatrix}\right] \quad (4)$$

where k_1 and k_2 present the corresponding wave vector at the Fermi energy with a momentum offset $\Delta k = k_2 - k_1$. Therefore, the spin expectation in the transport process is obtained as

$$\langle S_c(\boldsymbol{k})\rangle^+ = \begin{pmatrix}0\\ \sin(\Delta k y)\\ \cos(\Delta k y)\end{pmatrix} \quad (5)$$

dx.doi.org/10.1021/nl4027346 | Nano Lett. 2013, 13, 5264−5270

In other words, the spin vector will precess clockwise with the electron transport. On the contrary, by switching the direction of the electric field, the Rashba splitting contributed by another BiS_2 layer emerges at the Fermi level. As a result, the spin orientations of both inner and outer branch are reversed and the spin precession becomes counterclockwise

$$\langle S_c(\boldsymbol{k})\rangle^- = \begin{pmatrix} 0 \\ -\sin(\Delta ky) \\ \cos(\Delta ky) \end{pmatrix} \quad (6)$$

Considering the spin polarization of the analyzer pointing in the $+x$ direction and a total spin rotation of $\Delta ky_0 = \pi/2$, the carriers under positive E_{ext} can easily enter the analyzer (on-state), while the carriers under negative E_{ext} are significantly surpressed (off-state). By shifting the Fermi level under the degenerate point at X, like the green dashed line in Figure 3a, we have spin splitting hole carriers with the almost unchanged momentum offset $\Delta k = 2k_R = 0.05$ Å^{-1}. Therefore, we estimate the channel length y_0 to be about 3 nm, which is quite below the tolerance of the coherent transport in semiconductors. It is noticeable that the effect of the gates here is separating the coupled Rashba branches as well as moving the Fermi level properly to cross one branch to get the Rashba momentum offset, other than tuning the Rashba parameter in the Datta-Das SFET.[4] As described above, the Rashba parameter cannot be effectively tuned by the gate voltages. Consequently, the channel length has to be much longer to achieve a spin precession with the phase shift of π, which gives more chance to the spin diffusion and relaxation. According to the much better performance than the conventional SFET models, we expect our SFET model to be exploited for novel spintronic devices.

A similar electric control of spin splitting was also reported in the ferroelectric material GeTe for its tunability of the atomic position under an electric field.[15] However, the covalent bonding in GeTe limits its application in spintronics as thin films. Moreover, the electric control of ferroelectric polarization still remains a challenge itself. Here we propose another kind of electric modulation by selecting one helical spin state from two Rashba splittings from such a RL-BL-RL system, which also paves a new avenue for centrosymmetric materials as candidates for the next generation of spintronic devices.

In summary, by using relativistic first-principles calculations, we predict that 1-TL slab $LaOBiS_2$, which can form a stable 2D structure with the thickness only 1 nm, can produce two remarkable Rashba spin splittings and thus is desirable for the future SFET designs. There are three main reasons to ensure the large Rashba splitting in TL $LaOBiS_2$: (1) the "intercalation" La_2O_2 BL provides strong intrinsic polar electric fields to BiS_2 BLs, (2) the quantum barrier effect of La_2O_2 BL to protect two RLs from interacting with each other and preserve two counter-helical spin states, (3) the extra doubly degeneracy owing to the nonsymmophic character of the highly symmetric X point ensures band crossing in the Rashba bilayer system. The Rashba parameter can be effectively tuned by the intrinsic strain, while the bandgap and the helical direction of spin states sensitively depends on the external electric field. Finally, we improved the conventional Datta-Das SFET model by involving dual gates and the 2D $LaOBiS_2$ channel and confirm that a reasonable choice of the top and bottom gates corresponding to the channel length will achieve a good spin selecting performance, which benefits the future spintronic logic device.

Computational Methods. The electronic calculations were performed with the Vienna ab initio package (VASP).[43] The geometrical and electronic structures are calculated by the projector-augmented wave (PAW) pseudopotential[44] and the generalized gradient approximation of Perdew, Burke, and Ernzerhof (PBE) to the exchange-correlation functional.[45] The plane wave energy cutoff is set to 550 eV. Electronic energy minimization was performed with a tolerance of 10^{-4} eV, and all atomic positions were relaxed with a tolerance of 10^{-3} eV/Å. The lattice parameters are fully relaxed, and we get the lateral lattice constant a = 4.037 Å, which is quite similar to the bulk experimental value (4.05 Å).[46] The vacuum separation in the slab supercell is 20 Å to avoid the interaction between periodic images. Electric fields were applied normal to the 2D plane in VASP, which accomplishes this by introducing dipolar sheets at the center of the simulation cell.

The phonon calculations are carried out in density functional perturbation theory (DFPT) implemented in the CASTEP code.[47,48] The norm-conserving pseudopotential generated with the OPIUM code[49] is used with a k-point mesh of 6 × 6 and cutoff energy of 700 eV in the primitive cell. The exchange-correlation is also described by the PBE form.

AUTHOR INFORMATION

Corresponding Author

*E-mail: qihang.liu@northwestern.edu.

Notes

The authors declare no competing financial interest.

ACKNOWLEDGMENTS

We thank Kanber Lam from Northwestern University and Professor Stewart Clark of Durham University for the useful scripts and illuminating discussions. This research used resources of the National Energy Research Scientific Computing Center, which is supported by the Office of Science of the U.S. Department of Energy. This work is supported by "Center for Inverse design", a DOE Energy Frontier Research Center.

REFERENCES

(1) Kato, Y.; Myers, R. C.; Gossard, A. C.; Awschalom, D. D. *Nature* **2004**, *427*, 50−53.

(2) Meier, L.; Salis, G.; Shorubalko, I.; Gini, E.; Schon, S.; Ensslin, K. *Nat. Phys.* **2007**, *3*, 650−654.

(3) Bychkov, Y. A.; Rashba, E. I. *JETP Lett.* **1984**, *39*, 78−81.

(4) Datta, S.; Das, B. *Appl. Phys. Lett.* **1990**, *56*, 665−667.

(5) Lommer, G.; Malcher, F.; Rossler, U. *Phys. Rev. Lett.* **1988**, *60*, 728−731.

(6) Nitta, J.; Akazaki, T.; Takayanagi, H.; Enoki, T. *Phys. Rev. Lett.* **1997**, *78*, 1335−1338.

(7) LaShell, S.; McDougall, B. A.; Jensen, E. *Phys. Rev. Lett.* **1996**, *77*, 3419−3422.

(8) Koroteev, Y. M.; Bihlmayer, G.; Gayone, J. E.; Chulkov, E. V.; Blugel, S.; Echenique, P. M.; Hofmann, P. *Phys. Rev. Lett.* **2004**, *93*, 046403.

(9) Kimura, A.; Krasovskii, E. E.; Nishimura, R.; Miyamoto, K.; Kadono, T.; Kanomaru, K.; Chulkov, E. V.; Bihlmayer, G.; Shimada, K.; Namatame, H.; Taniguchi, M. *Phys. Rev. Lett.* **2010**, *105*, 076804.

(10) Ast, C. R.; Henk, J.; Ernst, A.; Moreschini, L.; Falub, M. C.; Pacile, D.; Bruno, P.; Kern, K.; Grioni, M. *Phys. Rev. Lett.* **2007**, *98*, 186807.

(11) Sakamoto, K.; Kakuta, H.; Sugawara, K.; Miyamoto, K.; Kimura, A.; Kuzumaki, T.; Ueno, N.; Annese, E.; Fujii, J.; Kodama, A.;

Shishidou, T.; Namatame, H.; Taniguchi, M.; Sato, T.; Takahashi, T.; Oguchi, T. *Phys. Rev. Lett.* **2009**, *103*, 156801.
(12) Gierz, I.; Suzuki, T.; Frantzeskakis, E.; Pons, S.; Ostanin, S.; Ernst, A.; Henk, J.; Grioni, M.; Kern, K.; Ast, C. R. *Phys. Rev. Lett.* **2009**, *103*, 046803.
(13) Ishizaka, K.; Bahramy, M. S.; Murakawa, H.; Sakano, M.; Shimojima, T.; Sonobe, T.; Koizumi, K.; Shin, S.; Miyahara, H.; Kimura, A.; Miyamoto, K.; Okuda, T.; Namatame, H.; Taniguchi, M.; Arita, R.; Nagaosa, N.; Kobayashi, K.; Murakami, Y.; Kumai, R.; Kaneko, Y.; Onose, Y.; Tokura, Y. *Nat. Mater.* **2011**, *10*, 521−526.
(14) Sakano, M.; Bahramy, M. S.; Katayama, A.; Shimojima, T.; Murakawa, H.; Kaneko, Y.; Malaeb, W.; Shin, S.; Ono, K.; Kumigashira, H.; Arita, R.; Nagaosa, N.; Hwang, H. Y.; Tokura, Y.; Ishizaka, K. *Phys. Rev. Lett.* **2013**, *110*, 107204.
(15) Di Sante, D.; Barone, P.; Bertacco, R.; Picozzi, S. *Adv. Mater.* **2013**, *25*, 509−513.
(16) Sakano, M.; Miyawaki, J.; Chainani, A.; Takata, Y.; Sonobe, T.; Shimojima, T.; Oura, M.; Shin, S.; Bahramy, M. S.; Arita, R.; Nagaosa, N.; Murakawa, H.; Kaneko, Y.; Tokura, Y.; Ishizaka, K. *Phys. Rev. B* **2012**, *86*, 085204.
(17) Eremeev, S. V.; Nechaev, I. A.; Koroteev, Y. M.; Echenique, P. M.; Chulkov, E. V. *Phys. Rev. Lett.* **2012**, *108*, 246802.
(18) Novoselov, K. S.; Geim, A. K.; Morozov, S. V.; Jiang, D.; Zhang, Y.; Dubonos, S. V.; Grigorieva, I. V.; Firsov, A. A. *Science* **2004**, *306*, 666−669.
(19) Cahangirov, S.; Topsakal, M.; Aktürk, E.; Şahin, H.; Ciraci, S. *Phys. Rev. Lett.* **2009**, *102*, 236804.
(20) Kane, C. L.; Mele, E. J. *Phys. Rev. Lett.* **2005**, *95*, 226801.
(21) Min, H.; Hill, J. E.; Sinitsyn, N. A.; Sahu, B. R.; Kleinman, L.; MacDonald, A. H. *Phys. Rev. B* **2006**, *74*, 165310.
(22) Liu, C.-C.; Feng, W.; Yao, Y. *Phys. Rev. Lett.* **2011**, *107*, 076802.
(23) Ni, Z.; Liu, Q.; Tang, K.; Zheng, J.; Zhou, J.; Qin, R.; Gao, Z.; Yu, D.; Lu, J. *Nano Lett.* **2011**, *12*, 113−118.
(24) Cao, T.; Wang, G.; Han, W.; Ye, H.; Zhu, C.; Shi, J.; Niu, Q.; Tan, P.; Wang, E.; Liu, B.; Feng, J. *Nat. Commun.* **2012**, *3*, 887.
(25) Mak, K. F.; He, K.; Shan, J.; Heinz, T. F. *Nat. Nanotechnol.* **2012**, *7*, 494−498.
(26) Zeng, H.; Dai, J.; Yao, W.; Xiao, D.; Cui, X. *Nat. Nanotechnol.* **2012**, *7*, 490−493.
(27) Mizuguchi, Y.; Demura, S.; Deguchi, K.; Takano, Y.; Fujihisa, H.; Gotoh, Y.; Izawa, H.; Miura, O. *J. Phys. Soc. Jpn.* **2012**, 81.
(28) Usui, H.; Suzuki, K.; Kuroki, K. *Phys. Rev. B* **2012**, *86*, 220501.
(29) Li, B.; Xing, Z. W.; Huang, G. Q. *Euro Phys. Lett.* **2013**, *101*, 47002.
(30) Wan, X.; Ding, H.-C.; Savrasov, S. Y.; Duan, C.-G. *Phys. Rev. B* **2013**, *87*, 115124.
(31) Yildirim, T. *Phys. Rev. B* **2013**, *87*, 020506.
(32) Ataca, C.; Şahin, H.; Ciraci, S. *J. Phys. Chem. C* **2012**, *116*, 8983−8999.
(33) Ataca, C.; Ciraci, S. *J. Phys. Chem. C* **2011**, *115*, 13303−13311.
(34) Das, T.; Balatsky, A. V. *Nat. Commun.* **2013**, 4.
(35) Nakosai, S.; Tanaka, Y.; Nagaosa, N. *Phys. Rev. Lett.* **2012**, *108*, 147003.
(36) Winkler, R. *Phys. Rev. B* **2004**, *69*, 045317.
(37) Zhang, Z.; Guo, W. *Phys. Rev. B* **2008**, *77*, 075403.
(38) Liu, Q.; Li, L.; Li, Y.; Gao, Z.; Chen, Z.; Lu, J. *J. Phys. Chem. C* **2012**, *116*, 21556−21562.
(39) Slomski, B.; Landolt, G.; Bihlmayer, G.; Osterwalder, J.; Dil, J. H. *Sci. Rep.* **2013**, 3.
(40) Bahramy, M. S.; Yang, B. J.; Arita, R.; Nagaosa, N. *Nat. Commun.* **2012**, 3.
(41) Bahramy, M. S.; Arita, R.; Nagaosa, N. *Phys. Rev. B* **2011**, *84*, 041202.
(42) Zhang, Y.; Tang, T.-T.; Girit, C.; Hao, Z.; Martin, M. C.; Zettl, A.; Crommie, M. F.; Shen, Y. R.; Wang, F. *Nature* **2009**, *459*, 820−823.
(43) Kresse, G.; Furthmüller, J. *Comput. Mater. Sci.* **1996**, *6*, 15−50.
(44) Kresse, G.; Joubert, D. *Phys. Rev. B* **1999**, *59*, 1758−1775.
(45) Perdew, J. P.; Burke, K.; Ernzerhof, M. *Phys. Rev. Lett.* **1996**, *77*, 3865−3868.
(46) Tanryverdiev, V. S.; Aliev, O. M.; Aliev, I. I. *Inorg. Mater.* **1995**, *31*, 1497.
(47) Clark, S. J.; Segall, M. D.; Pickard, C. J.; Hasnip, P. J.; Probert, M. I. J.; Refson, K.; Payne, M. C. *Z. Kristallogr.* **2005**, *220*, 567−570.
(48) Refson, K.; Tulip, P. R.; Clark, S. J. *Phys. Rev. B* **2006**, *73*, 155114.
(49) Rappe, A. M.; Rabe, K. M.; Kaxiras, E.; Joannopoulos, J. D. *Phys. Rev. B* **1990**, *41*, 1227.